CONFOCAL MICROSCOPIC IMAGE SEQUENCE COMPRESSION USING VECTOR QUANTIZATION AND 3D PYRAMIDS

W. Paul Cockshott, Yegang Tao, Gang Gao

Department of Computing Science
University of Glasgow
Glasgow, Scotland
wpc, tao, gaog@dcs.gla.ac.uk

Craig Daly

Faculty of Biomedical & Life Sciences
University of Glasgow
Glasgow, Scotland
c.daly@bio.gla.ac.uk

ABSTRACT

The 3D pyramid compressor project at the University of Glasgow has developed a compressor for images obtained from CLSM device. The proposed method using a combination of image pyramid coder and vector quantization techniques has good performance at compressing confocal volume image data. An experiment was conducted on several kinds of CLSM data using the presented compressor compared to other well-known volume data compressors, such as MPEG-1. The results showed that the 3D pyramid compressor gave higher subjective and objective quality of reconstructed images at the same compression ratio and presented more acceptable results when applying image processing filters on reconstructed images.

1. INTRODUCTION

The 3D pyramid compressor project at the University of Glasgow was funded by the Scottish Enterprise with a scheme of Proof of Concept Awards. The objective of this project is to provide a 3D compressor for confocal microscopic images. The basic concept of the 3D compressor is to read a stack of two-dimensional images, for example, a stack of microscopic images, sequentially into a three-dimensional array and compress the three-dimensional array. Here, we present a technique combining *vector quantization* (VQ) with a 3D differential image pyramid data structure for volume image data compression.

Confocal laser scanning microscopy (CLSM; single photon microscopy) has been available to biomedical scientists for almost 20 years [13]. However, it is only very recently that affordable computer power has enabled biologists to fully exploit the data contained within the large ($>$ 100Mb) image volumes. In this study we have used CLSM to collect 3D volumetric data describing the cellular organization and receptor protein distribution through the vascular wall of small segments of human and rat arteries. Briefly, arterial segments are stained with fluorescent markers for the cell nucleus (propidium iodide 1ug/ml) or beta-adrenergic receptors (BODIPY CGP12177, 0.1-1uM). Tissues are then slide mounted on the stage of either a NORAN (nuclear work) or Leica (receptor work) CLSM. Serial optical sections (x, y plane) are collected at intervals of 1um down through the axial plane (z-axis) to produce a 'stack' of optical planes which can be processed as a 3D volume. Processing, analysis and transfer of the resulting data volumes is time consuming and therefore a robust non-lossy or low distortion lossy compression routine would be of great value for biomedical purpose, e.g. in studying vascular structure [14]. Furthermore, the emergence of multi-photon microscopy as a practical laboratory tool now enables even greater depth penetration within thick biological samples. This coupled with studies involving multiple fluorophores imaged over time results in the collection of data sets approaching 1Gb per experiment. Thus, the need for efficient compression becomes even more important.

In 3D microscopy the raw data correspond to tracer densities at sub volumes in a 3D grid, with the size of the sub volumes constrained by the microscopy optics. The data is typically digitized as a sequence of 2D images, but this is an artificial presentation, inherently the data is 3 dimensional. This contrasts with the data in a movie sequence which is also captured as a sequence of 2D images, but in this case the generating physical process is 3D surfaces moving in time, which are then projected onto the 2D image plane of the camera. Because of this, we hypothesise that the higher order statistics of 3D microscopy data will differ from those of film. In particular planar motion normal to the camera axes - which motion compensation algorithms capture - has no corresponding generating physical process in microscopy. We thus hypothesise that the optimal compression strategy will differ from that used in film and video applications.

In this paper, we describe the use of 3D pyramid data structures to compress microscopy data. These exploit the inherent redundancy associated with correlation between tracer densities in 3 dimensions. We describe experimental results on several kinds vascular structural data. We compare the image quality with video coders currently in use. Finally, a brief conclusion is given in section V.

2. PREVIOUS WORK

2.1. Image Pyramid

Image pyramid data structures were originally developed for 2D image lossless coding. In this data structure, a *differential pyramid* (DP) is generated from an *image pyramid* (IP), which provides a multi-resolution model of image. In the image pyramid, an image is filtered producing a series of levels of images. The higher the level of image pyramid, the lower the resolution presented (see Fig. 1-a) [8, 9]. The scale factor for shrinking is usually 4. F_{shrink} and F_{expand} are two image scale transformation filters, where F_{shrink} decreases the image size and F_{expand} enlarges the image size. Many interpolation methods can be used for these two transformations, such as *nearest neighbor*, *bilinear*

and *bi-cubic*. Image pyramid provides a reasonable solution for progressive transmission of images: the top level will be transmitted first to reconstruct the image with lowest resolution, and the following levels will refine the reconstructed image stage by stage.

The differential pyramid is computed from the image pyramid to exploit the redundancy between each level of the image pyramid, and provides more efficient representation for transmission when combined with entropy coding. Fig. 1-b illustrates the construction of the differential pyramid. Suppose a IP and a DP with N-levels, we can formulate the construction as follows:

$$IP_i = \begin{cases} original\,image & i = N-1 (bottom) \\ F_{shrink}(IP_{i+1}) & i = N-2, \cdots, 0 \end{cases} \quad (1)$$

$$DP_i = \begin{cases} IP_i & i = 0 (top) \\ IP_i - F_{expand}(IP_{i-1}) & i = 1, \cdots, N-1 \end{cases} \quad (2)$$

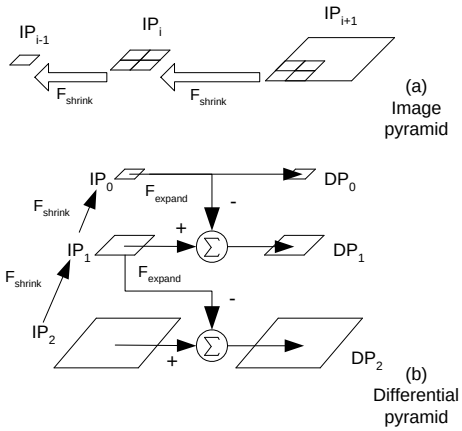

Fig. 1. Image pyramid and differential pyramid compositions.

Image pyramid is an redundant subband decomposition. That means the decomposed subbands need more storage requirement than the original image. Given L as the pyramid level, and s as the scale factor, number of pixels in pyramid will be

$$\begin{aligned} &NumOfPixels_{pyramid} \\ &= (1 + \tfrac{1}{s} + \tfrac{1}{s^2} + \cdots + \tfrac{1}{s^{L-1}}) NumOfPixel_{original} \\ &= (\tfrac{s^L - 1}{s^L - s^{L-1}}) NumOfPixel_{original} \end{aligned} \quad (3)$$

when compared with that of the original image. For instance, given $L = 5$ and $s = 4$, theres nearly 0.332 times of extra pixels in pyramid. However, since the histogram of the DP, as in lossless DPCM, is highly peaked around zero, some advanced entropy coding can take advantages of this.

2.2. Burt's Pyramid Coder

In 1983, Burt and Adelson introduced quantization into the image pyramid structure and proposed a multi-resolution lossy compression technique [8]. Using a scalar quantizer, only the pixels with high energy are transmitted to the decoder side, and the entropy can be substantially reduced by quantizing the pixel values in each level of the differential pyramid. Fig. 2 illustrates the block diagram of Burt and Adelsons pyramid coder. Their method,

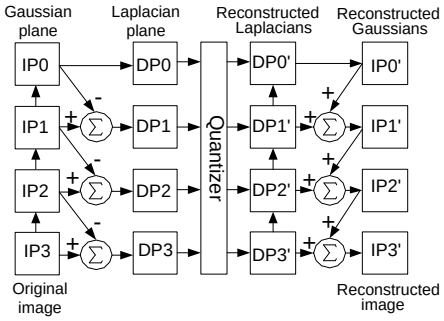

Fig. 2. Block diagram of Burt's pyramid coder.

introducing quantization into a pyramid structure has certain disadvantage. The quantization errors from upper levels would be magnified as they propagate down the pyramid during reconstruction. For example, an error affecting one pixel at the top of a three-level pyramid ends up corrupting sixteen pixels at the bottom layer. This disadvantage means Burt and Adelsons pyramid coding model doesn't give good results under high compression ratios, since increased errors are introduced when we set fewer quantization levels. In the next section, we extend the Burts pyramid by introducing vector quantization when constructing the differential pyramid with quantization noise feedback.

3. PROPOSED 3D PYRAMID CODER

3.1. 3D Pyramid Structure

The 3D version of our algorithm is used to compress the sequence of slices obtained from CLSM device. Unlike other 3D image data, e.g. video sequence, each frame in the CLSM sequence presents one slice of an object at specific depth. The 3D pyramid coder treats the whole sequence as a 3D volume data and exploits the multi-dimensional redundancy with only one procedure.

In Fig. 3, we gave an example of building a four-level 3D pyramid with VQ introduced. Wherein we generalize the F_{shrink} and F_{expand}, previously used on 2D image data, to 3D voxel data. Each voxel of level n maps to 8 voxels at level $n+1$. We can formulate the construction of 3D pyramid as follows (refer to Formula (1)-(2)):

$$IP_i = \begin{cases} original\,image & i = N-1 (bottom) \\ F_{shrink}(IP_{i+1}) & i = N-2, \cdots, 0 \end{cases} \quad (4)$$

$$DP'_i = VQ^{-1}(VQ(DP_i)) \quad i = 1, \cdots, N-1 \quad (5)$$

$$IP'_i = \begin{cases} IP_i & i = 0 (top) \\ DP'_i + F_{expand}(IP_{i-1}) & i = 1, \cdots, N-1 \end{cases} \quad (6)$$

$$DP_i = \begin{cases} IP_i & i = 0 (top) \\ IP_i + F_{expand}(IP'_{i-1}) & i = 1, \cdots, N-1 \end{cases} \quad (7)$$

There are several advantages of 3D pyramid structures. Firstly, they organize sequential images as 3D volume data. This can capture the correlation in 3 rather than 2 spatial dimensions. Another advantage is that although the 3D pyramid structure, like the 2D pyramid is redundant, when F_{shrink} and F_{expand} are applied to 3D volume data, the scale factor in formula (3) would be 8, not 4.

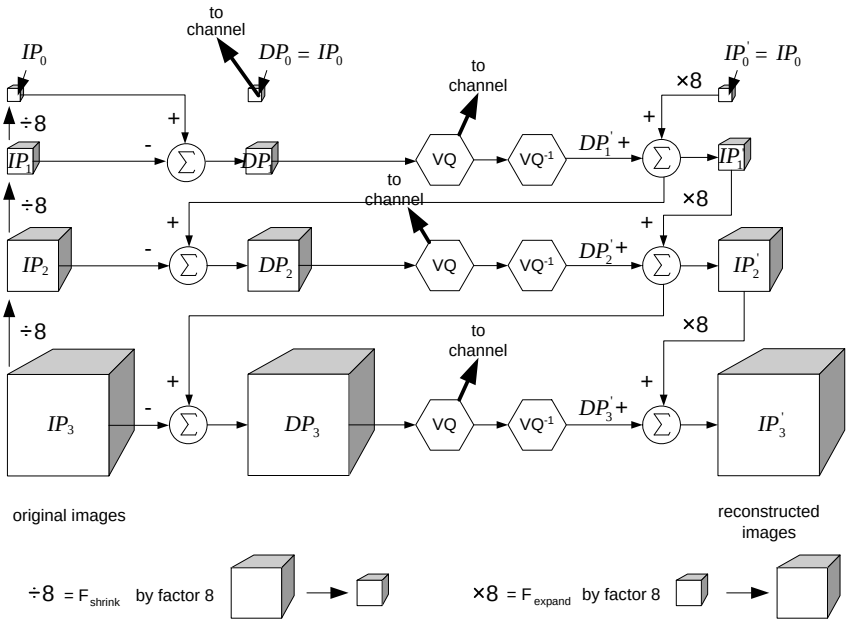

Fig. 3. Architecture of proposed compression technique using VQ with 3D image pyramid.

As a result the redundancy is only 1/7 rather than 1/3 for the 2D case.

3.2. Vector Quantizing Differential Pyramid

Vector quantization is an efficient technique for image compression [2, 3, 6]. It encodes a group of neighboring pixels together rather than individual pixel in scalar quantization. Since the neighboring pixels from an image are strongly correlated, according to Shannons rate-distortion theory [1], a better performance is achievable by coding vectors instead of scalars.

In a 3D pyramid, the output of the differential pyramid could either be scalar or vector quantized, we chose VQ rather than scalar quantization because of the higher compression ratio obtained at the same image quality. We use VQ to exploit the 3D correlations between voxels from intra-bands. The choise of intra-band coding rather than intre-band coding is based on the observation that the intra-band models capture most of the dependencies between the subbands coefficients, then exploiting intra-band redundancies offers a better coding gain than exploiting inter-band redundancies [6, 7]. The shape of a vector is specified by its *width*, *height* and *depth*. For instance, in Fig. 4, we construct an eight-dimensional vector $2 \times 2 \times 2$ $(w \times h \times d)$ by sampling four neighboring pixels from frame i and four neighboring pixels at the same position from its next frame $i + 1$. The shapes we typically use are $2 \times 2 \times 2$ or $4 \times 4 \times 2$, but the choice is programmable. In experiment, we observed that, for some image stacks like BxCGP/BxCGS, higher image quality can be achieved using vectors having larger size along the depth axis than that along planar axes, such that vectors of shape $2 \times 1 \times 4$ are preferable to those of shape $2 \times 2 \times 2$. This is based on the fact that for these stacks, correlation in depth direction is higher than in planar direction, for reasons pertaining to microscope optics.

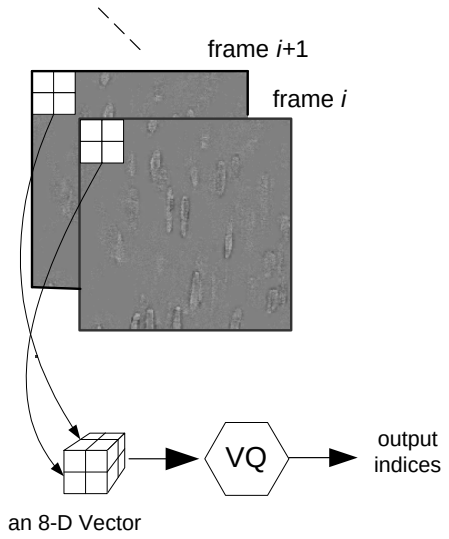

Fig. 4. An example of forming an intra-band vector from two successive frames.

3.3. Thresholding

The thresholding algorithm is based on two important observations:

1. Differential images in pyramid have the characteristics that most of the coefficients energies are concentrated around

zero (see Fig. 4[1]).

2. The coefficients with larger magnitude (high energy) are more important than smaller magnitude coefficients (low energy) because they contribute more to the decreasing of distortion after receiving by decoder.
3. When an image is pyramid decompositioned the energy in subbands increases as the resolution decreases, so the coefficients will, on average, be smaller in lower pyramid level than in the higher pyramid level.

These first two observations are exploited by the thresholding scheme by discarding a large part of the low energy blocks to yield a data stream suitable for entropy encoding. Assuming we have a codebook matrix M with n rows, and each row represents a code vector. When designing a codebook there will always be a vector in the codebook matrix with a minimum energy. In what follows we will assume that the codebooks are so designed that the minimum energy vector actually has zero energy. That is to say all elements are zero. We call this vector Z, and assuming it is the z-th row in codebook matrix. The thresholding algorithm scans each index i from the encoder and checks if $\mid M_i \mid^2 > T$ where T is some energy threshold. If the answer is positive, the i is transmitted to the entropy encoder. Otherwise, the index i is replaced by z, which is the index of Z, before being transmitted to the decoder. An entropy encoder such as LZ, or a Huffman codec is placed downstream from the vector quantizer so that the vector quantizer data stream is, in most cases, mapped to a shorter bit stream containing the same information content. A corresponding LZ or Huffman codec is used at the decoder side to reconstruct the VQ data stream.

According to the third observation, T is individual in each layer. We discard more coefficients from lower pyramid levels by assigning larger thresholding values.

4. EXPERIMENTAL RESULTS

We have performed coding experiments on two kinds of grey scale CLSM image volumes with 8 bits per pixel, which captured by the *EC FP5* partnership for vascular imaging (VASCAN 2000). The first data sets from rat mesenteric artery are stained with BODIPY CGP12177, which attaches to beta-adrenergic receptors. Therefore, the data sets show the distribution of CGP binding sites. On the outside of the vessel one can see the drug binding to adventitial cells and nerves. In the middle one can see binding to the smooth muscle cells. Human resistance artery data show DNA staining. Therefore, only the nucleus of each cell is visible. The long thin nuclei are located within smooth muscle cells. Irregular shaped nuclei near the surface are within adventitial cells. Elongated nuclei deep within the volume are within endothelial cells. Table 2 describes these data sets.

4.1. Rate-distortion performance

We tested the rate-distortion (R/D) performance of a 3D pyramid compressor and listed the result in Table 1. The data sets of human resistance arteries have many regions, in which there are very low variations between voxels. We can get compression ratio as high as about 150:1 on these data sets. Data sets of rat mesenteric artery have much more details. We can get about $15 \sim 20 : 1$ compression ratio on these data sets with acceptable image quality. The *Peak-Signal-to-Noise Ratio (PSNR)* measure used in the table is defined by

$$PSNR = 10 \log_{10} \frac{255^2}{MSE} \tag{8}$$

where MSE is the mean-squared-error between the original and reconstructed images.

Table 2. Description of CLSM data

Filename	Description	Volume size (voxels)	Data size (bytes)
B1CGS	Rat mesenteric artery	$256 \times 256 \times 168$	11,303,376
B3CGP		$256 \times 256 \times 178$	11,976,196
B4CGS		$256 \times 256 \times 170$	11,445,476
B6CGS		$256 \times 256 \times 183$	12,320,285
G25_HG70	Human resistance arteries	$512 \times 512 \times 135$	35,523,360
G27_HG70		$512 \times 512 \times 89$	23,419,104

We compared the R/D performance of proposed 3D image coder with standard JPEG image coder to examine how much improvement we can obtain using 3D based methods rather than using 2D based ones. We fed two stacks B3CGP and G27_HG70 into JEPG coder, and we outputted the JPEG-coded images as the same quality as 3D pyramid-coded ones. For B3CGP stack, the output bit rate we achieved was 0.382 *bpp (bit-per-pixel)* using 3D pyramid, while was only 0.875 *bpp* using JPEG. For G27_HG70 stack, we achieved 0.084 *bpp* using 3D pyramid, which roughly the half size of the output bit rate as 0.156 *bpp* using JPEG.

We also compared the 3D pyramid method with two video compressors: MPEG-1 and Indeo©Video Codec 5.10. MPEG-1 uses *motion compensation* and *DCT* techniques [11, 12], while Indeo codec is based on *hybrid wavelet compression technology*. We used two data sets, one from rat mesenteric data and the other from artery human resistance arteries data. We specified the format of image sequences as 'gray scale' images when encoding using MPEG-1 and Indeo codecs. This guaranteed that no color information would be taken into account. The comparison results show that the proposed method offers better image quality than MPEG-1 and Indeo Codec 5.10 at almost the same compression ratio. Fig. 7 shows the compression results B3CGP rat mesenteric data sets. The average PSNR for the 3D pyramid method is roughly 0.11 dB and 1.70 dB better than that of MPEG-1 and Indeo. Fig. 7b-2 $\sim$ 4 gave the decompressed results of the 47^{th} frame using three codecs respectively. For 3D pyramid method, the histogram shows almost the same overall shape as in Fig. 7b-1, but smoothed, indicating that noise has been filtered out. However the jaggedness are not removed with other two codecs. Fig. 8 shows the compression result on G27_HG70 human resistance arteries data set. For this data set, we also get better image quality with the 3D Pyramid, with gains of 0.59 dB and 0.63 dB over MPEG-1 and Indeo. We recognized that for very low bit rate, the reconstructed images obtained by 3D pyramid scheme have blurring in some regions, while the images obtained by Indeo and MPEG-1 have blocking effects, which are more irritating to the human visual system(see Fig. 8b-2 $\sim$ 4). Another point worth mentioning is that while MPEG-1's coding rate varies with every frame, 3D pyramid scheme has a fixed rate allocation over whole stack, which makes the PSNR

[1]For illustration purpose, an offset of 128 has been added to every coefficient except those from top level. The zero-energy coeffiencts will be displayed as mid-gray.

Table 1. Performance of 3D Pyramid Compressor on 6 data-sets

Filename	Original data size (bytes)	Output data size (bytes)	Compression ratio (C/R)	Ave. PSNR (dB)	3D Pyramid specifications				
					Pyramid levels	Entries in codebook	Vector shape $(w \times h \times d)$	VQ training algorithm	Thresholds (different between layers)
B1CGS	11,303,376	712,666	15.86	30.8155	4	256	$2 \times 2 \times 3$	LBG [4]	top - 0:0:1:4 - bottom
B3CGP	11,976,196	566,132	21.15	33.2712	4	256	$2 \times 2 \times 3$	LBG	0:0:2:7
B4CGS	11,445,476	608,267	18.82	33.5211	4	256	$2 \times 2 \times 3$	LBG	0:0:1:4
B6CGS	12,320,285	750,093	16.43	31.8014	4	256	$2 \times 2 \times 3$	LBG	0:0:1:4
G25_HG70	35,523,360	211,152	168.24	35.3181	5	256	$4 \times 4 \times 4$	LBG	0:0:1:4:16
G27_HG70	23,419,104	246,371	95.06	35.7988	5	256	$4 \times 4 \times 3$	LBG	0:0:0:2:8

curves of 3D pyramid more smooth than that of MPEG-1.

4.2. Image processible performance

Microscopists need image processing techniques as useful tools for multiple purpose analysis. Post-processing results on decompressed data will be used as another criterion of a lossy coding technique.

In Fig. 8, we used *sobel* operators [10] to perform edge-detection on the decompressed images using 3D pyramid, MPEG-1 and Indeo codec respectively. The blocky artifacts introduced using MPEG-1 and Indeo codec affect the processing results seriously, making the nuclei hard to be distinguished from the muscle cells.

We set up another test to examine how much a codec will affect the measurements of interested areas (objects) on images. We choose the 41^{st} frame from the G27_HG70 data set. The shapes of nucleus of each cell in this image are what people interested [14]. We used Metamorph©, a powerful microscopy analysis tool from *Universal Imaging Corporation*, to do the measurements on five categories: Pixel area, Perimeter, Length, Breath, Shape factor. Fig. 5 shows the pre-processed raw image and its corresponding post-processed image. Given a specific thresholding, totally 25 objects have been recognized and measured.

We performed such measurements on the same frame from decompressed stacks coded by 3D pyramid, Indeo and MPEG-1 respectively. We illustrated the measurement results in Fig. 6. These results have been normalized by computing the ratio to the measurement results of raw image. In this test, 3D pyramid coded image gave the best results in that its measurements distributions were more consistent with those of raw image than other two codecs did. We noticed the blocking artifacts in Indeo and MPEG-1 coded images affected the measurement results seriously.

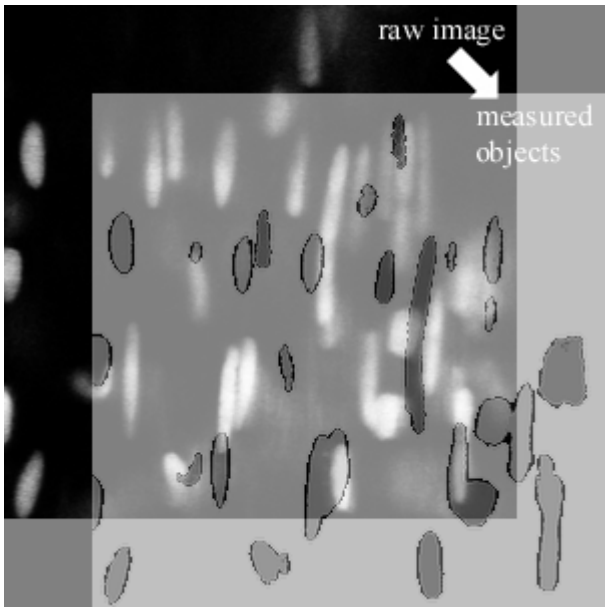

Fig. 5. Totally 25 objects have been recognized and measurements are performed on five categories: Pixel area, Perimeter, Length, Breath, Shape factor.

4.3. Computational expenses

We examined the computational expense of the proposed codec on these data sets. The settings of the coder follow the specifications in Table 1. We list the corresponding CPU times of encoding and decoding in Table 3. The proposed coder is asymmetry in that more computing time is required for encoding than for decoding. This is because the encoding process involves many computations for codebook training and searching, whereas the VQ decoder simply generates image blocks according to the codebook indexing information received. Such asymmetry would be suitable for reviewing purpose, which requires the fast reconstruction of images while not cares much about encoding speed.

Refer to Fig.3, we can view the encoding process as a series tasks. First of all, we construct the image pyramid by running filtering and subsampling operations from level to level. The CPU time is proportion to the size of data sets. The second task is training a codebook from the vector set sampled from the differential image pyramid. We choose LBG as the codebook training method to ensure a locally optimal result. The computational expense for this task is affected by two factors: the size of training set (number of vectors in training set) and the size of vector. When we obtained a well-trained codebook, we fed the differential pyramid into vector quantizer. The codebook was unstructured, then a full-search method was used for VQ encoding. Here, we used a fast search technique [5] for speeding the full search of an arbitrary codebook. In our experiments, this method reduced the computational complexity of nearest neighbor search from $O(k \times N^2)$ to roughly $O(k \times N)$ of a codebook containing N k-dimensional codevectors. The final task is reconstructing the image pyramid. Compared to Burts open-loop pyramid structure (see Fig.2), we build up a closed-loop pyramid. The quantization errors will be feedback to the encoder at the next pyramid level, which means the decoding process is included in the encoding process, so the reconstructing task in encoding process will be exactly the same as decoding process. This process includes the reconstruction of the differential pyramid and interpolation of the image pyramid from

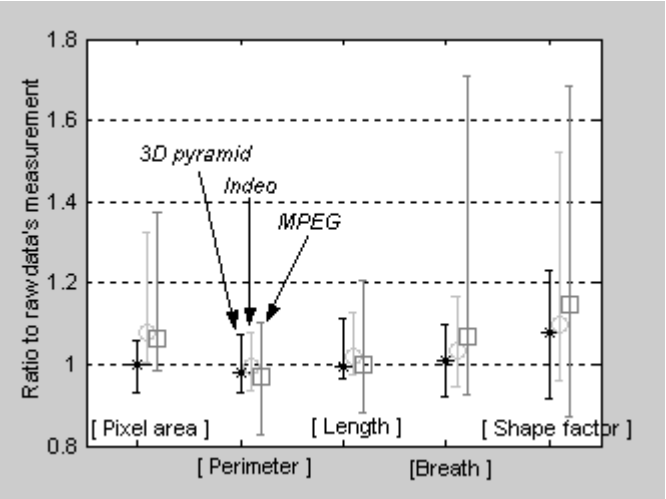

Fig. 6. Each bar illustrates the range and the mean of distribution of 25 measured data in each category. Data have been normalized by computing the ratio to the raw measurements.

Table 3. CPU Times to encode and decode testing data sets (Pentium III©1GHz)

Filename	Encode (s)				Decode (s)
	building image pyramid	codebook training (Num. of vectors in training set)	encoding differential pyramid	recon. image pyramid	
B1CGS	5.78	35.89 (49,384)	21.42	6.62	6.62
B3CGP	5.25	27.00 (35,360)	15.16	6.19	6.19
B4CGS	5.13	27.50 (35,787)	15.52	5.92	5.92
B6CGS	5.33	30.83 (44,548)	20.80	6.44	6.44
G25_HG70	13.07	83.14 (22,032)	26.81	14.97	14.97
G27_HG70	10.56	59.58 (20,546)	25.75	11.67	11.67

top level to bottom level, and the CPU time is mainly determined by interpolation operations because of the very low computational cost for decoding vector quantized data [3].

5. CONCLUSION

In this paper, a 3D lossy confocal microscopy image compression scheme, using 3D pyramid structures and vector quantization, is introduced. The 3D pyramid structures utilize the correlations between voxels in 3 spatial dimensions and decompose the source signal into a series of levels of subbands, which would be more suitable for quantization and entropy coding.

The experimental results show that the 3D pyramid method provides good qualities of reconstructed images at $15 \sim 20 : 1$ compression ratio on rat mesenteric data sets; and 100:1 or even higher compression ratio on human resistance arteries ones. Both offer better image quality than that using MPEG-1 and Indeo©Video codec 5.10 at the same compression ratios. The following image processing results on reconstructed images also show the 3D pyramid coder is more acceptable, especially for compressing volume data having low variation between voxels, like G27_HG70 stack, at high compression ratio.

6. REFERENCES

[1] C. E. Shannon. *Coding Theorems for a Discrete Source with a Fidelity Criterion.* IRE Convention Record, part 4, pp. 142-163, Mar. 1959.

[2] R.M. Gray, D.L. Neuhoff. *Quantization.* IEEE Trans. Inform., vol. 44(6), pp. 2325-2383, Oct. 1998.

[3] Nasser M. Nasrabadi, Robert A. King. *Image Coding Using Vector Quantization: A Review.* IEEE Trans. Commun., vol. 36(8), pp. 957-970, Aug. 1988.

[4] Y. Linde, A. Buzo, R. M. Gray. *An Algorithm for Vector Quantizer Design* IEEE Trans. Commun., vol. 28, pp. 84-95, Jan. 1980.

[5] M. R. Soleymani, S. D. Morgera. *An Efficient nearest neighbor search method* IEEE Trans. Commun., vol. 35, pp. 677-679, July 1987.

[6] P. Cosman, R. Gray, M. Vetterli. *Vector Quantization of Images Subbands: A Survey.* IEEE Trans. Image Processing, vol. 5, pp. 202-225, Feb. 1996.

[7] Peter Schelkens, *et. al. Wavelet Coding of Volumetric Medical Datasets.* IEEE Trans. Medical Imaging, special issue on wavelets in medical imaging.

[8] Peter J. Burt, Edward H. Adelson. *The Laplacian Pyramid as a Compact Image Code.* IEEE Trans. Commun., vol. 31, pp. 532-540, Apr. 1983.

[9] E.H. Adelson, C.H. Anderson, J.R. Bergen, P.J. Burt, J.M. Ogden. *Pyramid Methods in Image Processing.* RCA Engineer, vol. 29(6), Nov/Dec 1984.

[10] R. C. Gonzalez, R. E. Woods. *Digital Image Processing (2nd Edition).* Addison-Wesley Pub Co. ISBN: 0201180758.

[11] Barry G. Haskell, Atul Puri, Arun N. Netravali. *Digital Video: An Introduction to MPEG-2.* Kluwer Academic Publisher, 1997.

[12] Borko Furht, Joshua Greenberg, Raymond Westwater. *Motion Estimation algorithm for Video Compression.* Kluwer Academic Publishers, 1997.

[13] James B. Pawley. *Handbook of biological confocal microscopy (2nd Edition).* Plenum Press, 1995. ISBN: 0306448262.

[14] Craig Daly, *et. al. Analysing the 3D Structure of Blood Vessels using Confocal Microscopy.* Microscopy and Analysis (UK), vol. 92, pp. 5-8, 2002.

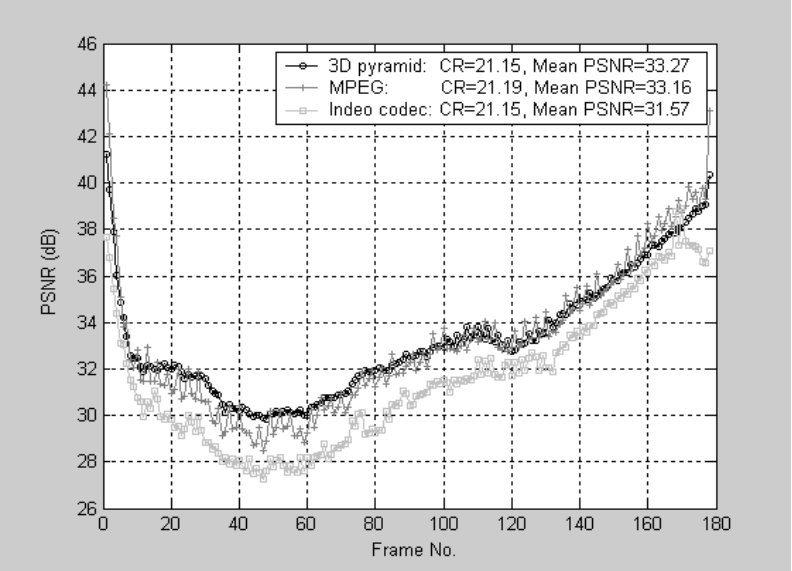

(a) Coding results using 3D pyramid method compared to MPEG and Indeo Video Codec 5.10 at the almost the same compression ratio (CR), Peak Signal to Noise Ratio (PSNR) for each frame.

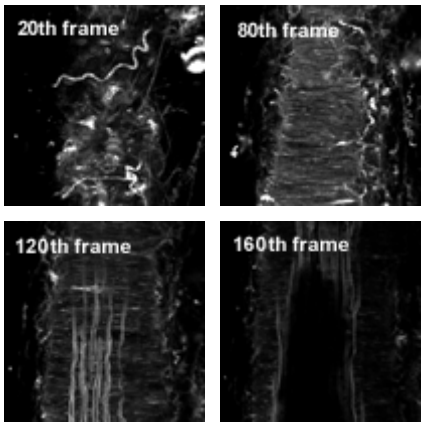

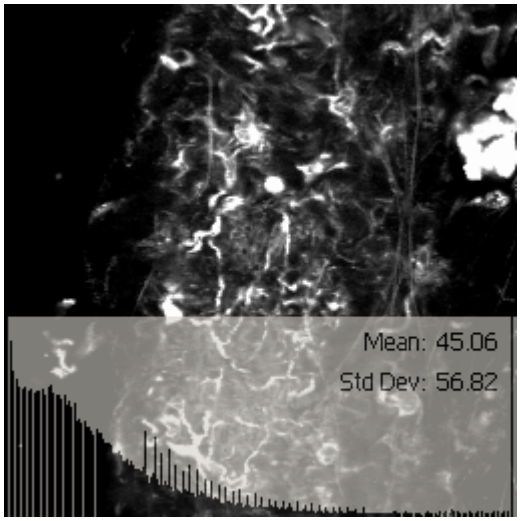

(b-1) The 47th frame from original image data set. The intensity histogram is superimposed on the lower part of the image. The histogram shows some jaggedness due to noise.

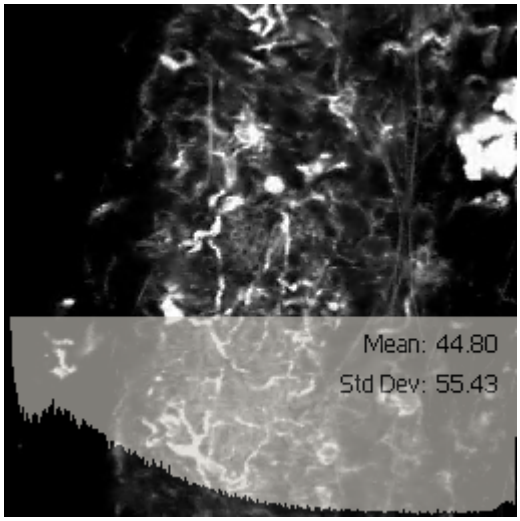

(b-2) The reconstructed image using 3D pyramid codec, PSNR = 29.88. There is no visible loss of quality; the histogram remains the same shape as the original but shows considerable smoothing.

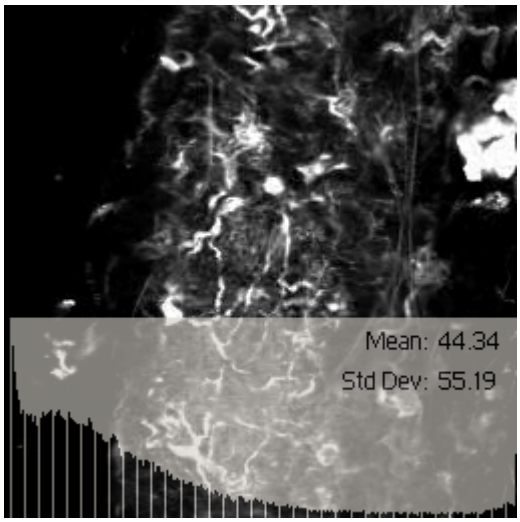

(b-3) The reconstructed image using MPEG video codec, PSNR = 28.50.

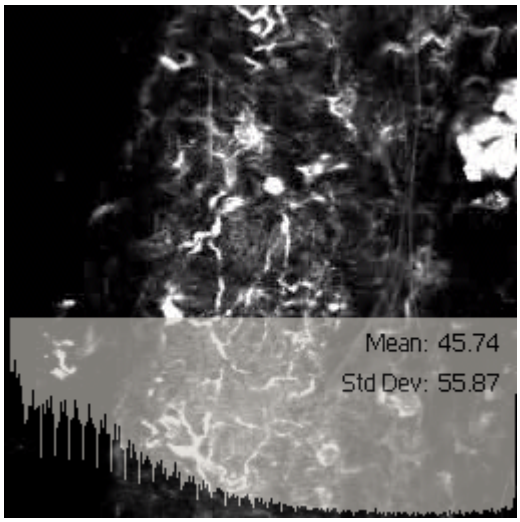

(b-4) The reconstructed image using Indeo© Video codec 5.10, PSNR = 27.24. The shape of histogram is biased from the original; the jaggedness still remain.

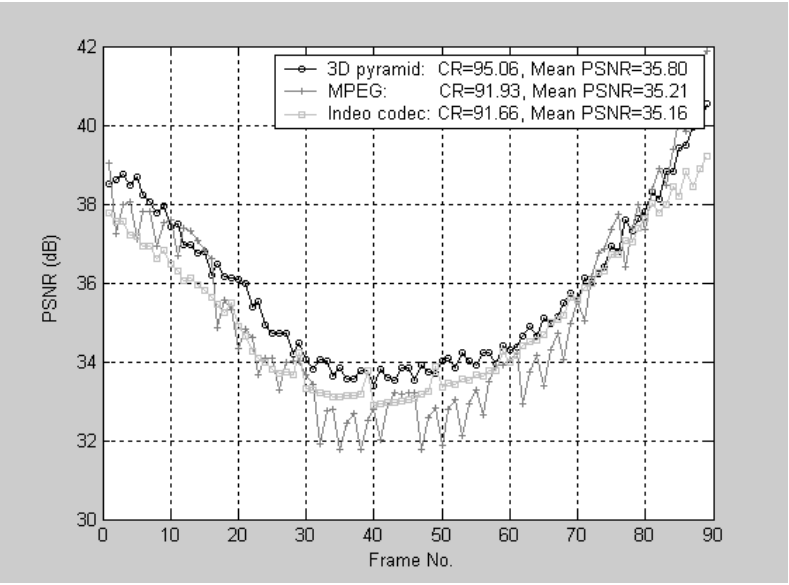

(a) Coding results using 3D pyramid method compared to MPEG and Indeo Video Codec 5.10 at the almost the same compression ratio (CR), Peak Signal to Noise Ratio (PSNR) for each frame.

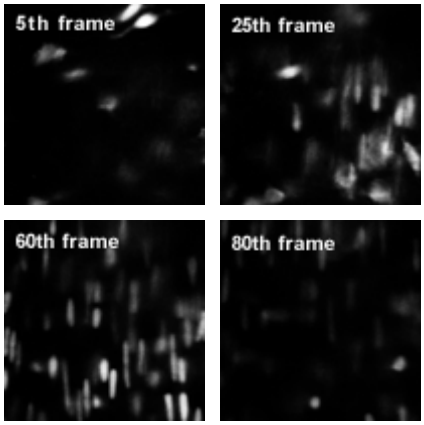

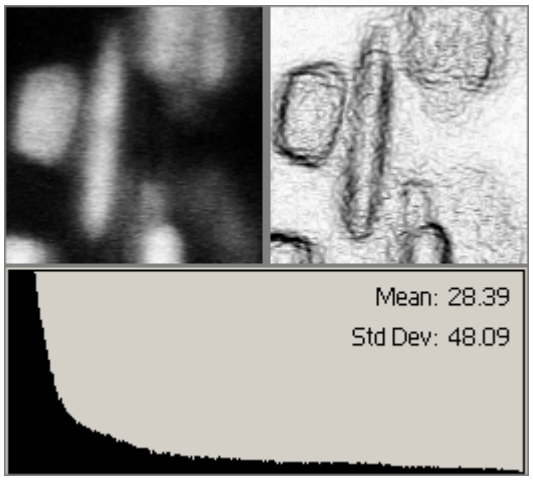

(b-1) An 128 x 128 area clipped from the 41st frame from original image data set as shown top left corner. The result of edge-detection filter is shown on its right side. The histogram of the entire frame is shown on the lower part.

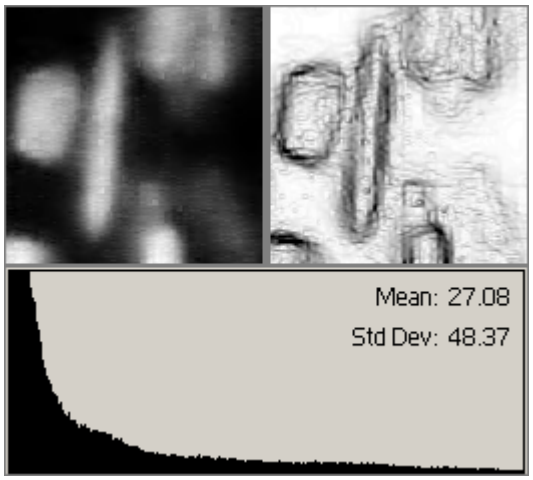

(b-2) The reconstructed image using 3D pyramid codec, PSNR = 33.76. The edge-detection result didn't affect by the compression.

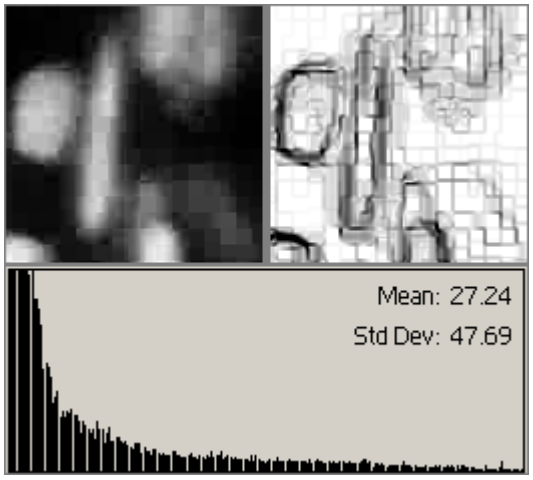

(b-3) The reconstructed image sequence using MPEG video codec, PSNR = 32.01. The blocky artifacts afftect the edge-detection result.

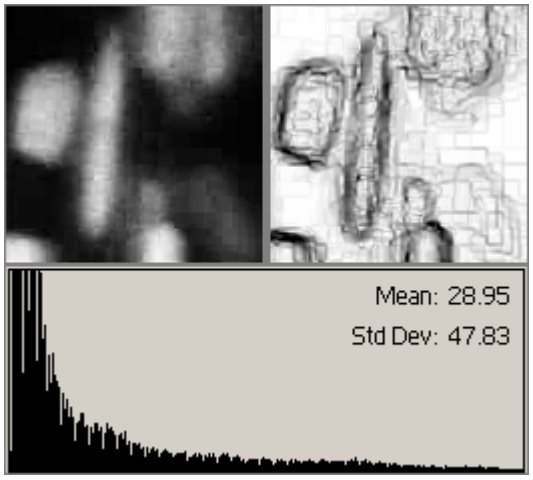

(b-4) The reconstructed image sequence using Indeo Video codec 5.10, PSNR = 32.91. Unexpected artifacts are also visible in decompressed image and its edge-detection result.